Available online at www.sciencedirect.com
SCIENCE DIRECT®
Journal of Magnetic Resonance 160 (2003) 13–19
JMR Journal of Magnetic Resonance
www.elsevier.com/locate/jmr

NMR second moment imaging using Jeener–Broekaert dipolar signals

S. Matsui,[a,*] S. Saito,[a] T. Hashimoto,[b] and T. Inouye[c]

[a] *Institute of Applied Physics, University of Tsukuba, Tsukuba, Ibaraki 305-8573, Japan*
[b] *Yokohama Soei College, Yokohama, Kanagawa 226-0015, Japan*
[c] *Institute for Applied Mathematics, Inc., Tsukuba, Ibaraki 305-0005, Japan*

Received 29 January 2002; revised 20 August 2002

Abstract

It is demonstrated that imaging of the ^{1}H NMR second moment can be achieved by using the Jeener–Broekaert (JB) dipolar signal instead of the Zeeman FID signal commonly employed. The JB dipolar signal can be induced by applying a JB pulse sequence, $90°_x$–τ – $45°_y$–τ' – $45°_y$, which is followed by the time-suspension magic echo sequence, TREV-16TS, for imaging detection. Scanning the imaging detection to cover the whole evolution of the JB dipolar signal finally results in producing spatially resolved JB dipolar signals. The local value of the quantity called the "JB second moment," $M_{2(\mathrm{JB})}$, is then estimated from the initial slope of each resolved JB dipolar signal. The $M_{2(\mathrm{JB})}$ can be regarded as the "weighted" powder average of the usual second moment. The "weighting" effect due to the JB sequence leads to the τ dependent $M_{2(\mathrm{JB})}$ value. The τ dependence is potentially useful for characterizing the second moment distribution resulting from the crystal orientation dependence: For example, in addition to the usual powder average, an approximate distribution range can be deduced by a simple analysis of the τ dependence, serving as a new contrast for materials imaging. This is illustrated by preliminary experiments performed on test samples.

Keywords: Second moment imaging; Jeener–Broekaert sequence; Dipolar signal; Orientation dependent second moment; Magic echo

1. Introduction

The Jeener–Broekaert (JB) sequence, $90°_x$–τ – $45°_y$–τ' – $45°_y$, is generally used for measuring the spin–lattice relaxation time, $T_{1\mathrm{D}}$, by creating ($90°_x$–τ – $45°_y$) dipolar order and then monitoring (τ' – $45°_y$) the decay of the order during the time interval τ' [1]. Here, the pulse spacing τ is usually set around the spin–spin relaxation time, T_2, for creating the order at a maximal efficiency of about 56%. For obtaining a better efficiency, the ADRF (Adiabatic Demagnetization in the Rotating Frame) technique [2] may be employed. When $T_{1\mathrm{D}}$ is not sufficiently long, however, the technically simpler JB sequence is often preferable, giving an eventually larger signal after the monitoring pulse.

The signal, $\langle I_y \rangle$, induced after the monitoring $45°_y$ pulse is referred to as the "dipolar signal," the intensity of which is proportional to the magnitude of the dipolar order created. Unlike the usual NMR signal, FID, observed by applying a 90° pulse in the presence of Zeeman order, the dipolar signal starts from "zero" and assumes an "echo-like shape" corresponding to the time derivative of the FID [1,2]. This is due to the fact that the net polarization of the dipolar order is zero, in contrast to that of the Zeeman order.

So far, NMR imaging experiments have generally been conducted by using the Zeeman signal. To our knowledge, no imaging experiment using the dipolar signal seems to have been reported. The peculiar "echo-like shape" of the dipolar signal has aroused our interest to use it for NMR imaging: The dipolar signal shape appears to expose the information of dipolar interaction more directly than the Zeeman signal shape. Here, we focus on the imaging experiment in which the

* Corresponding author. Fax: +81-298-53-5205.
E-mail address: matsui@bk.tsukuba.ac.jp (S. Matsui).

1090-7807/02/$ - see front matter © 2002 Elsevier Science (USA). All rights reserved.
PII: S1090-7807(02)00034-4

information of ^{1}H NMR second moment is extracted from the JB dipolar signal.

The second moment is a useful parameter for characterizing molecular mobility in solids. Compared to the second moment imaging experiments based on the Zeeman signal [3–5], the signal sensitivity is lost to some extent in the JB experiments because of the less efficient JB transfer of order from the Zeeman to the dipolar reservoir [1], and of the decay by the often fast T_{1D} relaxation. However, due to a "weighted" creation of dipolar order by the JB sequence, the use of JB dipolar signal allows a "weighted" powder average of the second moment to be obtained. It can yield more detailed information on the second moment than that obtained using the Zeeman signal.

2. Second moment imaging using the JB dipolar signal

It is well known that the Zeeman FID signal, $G(t)$, can be expanded in terms of the Van Vleck moments [6] such that

$$G(t) = G_0\left(1 - \frac{M_2 t^2}{2!} + \frac{M_4 t^4}{4!} - \frac{M_6 t^6}{6!} + \cdots\right), \tag{1}$$

where M_n ($n = 2, 4, 6, \ldots$) denotes the nth moment and G_0 is the initial amplitude of the FID. When the molecules undergo some motion, the nth moments, M_n, actually measured and hence the observed FID signal shape, $G(t)$, depend on the type and degree of the molecular motion. The lowest moment, M_2, is particularly useful for studying the molecular mobility. (Although the molecular motion leads to non-zero values for the odd moments, we assume that the odd moments are negligibly small in Eq. (1).) For calculating the second moment M_2 measured experimentally, it is necessary to use, instead of the rigid-lattice dipolar Hamiltonian, the effective dipolar Hamiltonian whose amplitude is reduced by the time averaging due to the molecular motion [6].

The previously reported methods of second moment imaging using the Zeeman signal [3–5] were based on Eq. (1). The second moment M_2 can be extracted from the initial curvature of the FID; namely,

$$M_2 = -\left|\lim_{t\to 0}\frac{\mathrm{d}^2 G(t)}{\mathrm{d}t^2}\right| \Big/ G_0. \tag{2}$$

In most imaging experiments of materials, the imaging object is usually orientationally disordered, i.e., a powder. In such a case, the observed Zeeman FID signal, $G(t)$, and the measured nth moments, M_n, in Eqs. (1) and (2) may be expressed by the corresponding powder averages [6]

$$G(t) = \frac{\int G^{\Omega}(t)\,\mathrm{d}\Omega}{\int \mathrm{d}\Omega} \tag{3}$$

and

$$M_n = \frac{\int M_n^{\Omega}\,\mathrm{d}\Omega}{\int \mathrm{d}\Omega}, \tag{4}$$

where $G^{\Omega}(t')$ and M_n^{Ω} represent, respectively, the FID and the nth moments obtained from a tiny single crystal having an orientation Ω with respect to the static magnetic field and $\int \mathrm{d}\Omega = \int\int \sin\theta\,\mathrm{d}\theta\,\mathrm{d}\phi$.

The expression for the JB dipolar signal, on the other hand, may be more complicated than that for the Zeeman signal. This is because the JB sequence, $90°_x$–$\tau - 45°_y$–$\tau' - 45°_y$–t, consists of the three RF pulses separated by the time intervals τ and τ' while the Zeeman FID signal can be induced by applying a single RF pulse. The original JB experiment was performed on the ^{19}F spin system in a CaF_2 single crystal with the (1 0 0) crystal axis aligned along the static magnetic field [1]. It shows that the JB dipolar signal can be given for the oriented (Ω) single crystal by [7]

$$S^{\Omega}(\tau,\tau',t) = S_A\left[\frac{1}{M_2^{\Omega}G_0}\frac{\mathrm{d}G^{\Omega}(\tau)}{\mathrm{d}\tau}\right] \times \exp\left[-\frac{\tau'}{T_{1D}^{\Omega}}\right]\left[\frac{1}{G_0}\frac{\mathrm{d}G^{\Omega}(t)}{\mathrm{d}t}\right]. \tag{5}$$

Here, the term $[(M_2^{\Omega}G_0)^{-1}\,\mathrm{d}G^{\Omega}(\tau)/\mathrm{d}\tau] \equiv E^{\Omega}(\tau)$ represents the efficiency of creating the dipolar order, the exponential term $\exp[-\tau'/T_{1D}^{\Omega}] \equiv R^{\Omega}(\tau')$ denotes the T_{1D}^{Ω} relaxation decay of the created order, the last term $[G_0^{-1}\,\mathrm{d}G^{\Omega}(t)/\mathrm{d}t]$ indicates the shape of the dipolar signal, and S_A is the amplitude of the created order that is proportional to G_0. We have assumed that G_0 and S_A are independent of the orientation Ω as usual. For an orientationally disordered sample, the powder average must be taken similarly as in Eq. (3)

$$S(\tau,\tau',t) = \frac{\int S^{\Omega}(\tau,\tau',t)\,\mathrm{d}\Omega}{\int \mathrm{d}\Omega}. \tag{6}$$

Due to the orientation dependence of the efficiency and relaxation terms, the expression for the powder-averaged JB dipolar signal $S(\tau,\tau',t)$ is complicated and the signal shape generally depends on τ and τ'.

We assume that the JB dipolar signal $S(\tau,\tau',t)$ can be expanded in terms of the JB moments such that

$$S(\tau,\tau',t) = S_A\tau\left(M_{2(JB)}t - \frac{M_{4(JB)}t^3}{3!} + \frac{M_{6(JB)}t^5}{5!} - \cdots\right), \tag{7}$$

where the nth JB moments, $M_{n(JB)}$, are not equivalent to the usual powder averages of the nth moments M_n^{Ω} but regarded as the "weighted" powder averages of M_n^{Ω} with the weighting factor given by the efficiency and relaxation terms $E^{\Omega}(\tau)$ and $R^{\Omega}(\tau')$ in Eq. (5). We define the nth JB moments by

$$M_{n(\mathrm{JB})} = \frac{\int \left[-E^{\Omega}(\tau)R^{\Omega}(\tau')/\tau \right] M_n^{\Omega}\, \mathrm{d}\Omega}{\int \mathrm{d}\Omega}. \tag{8}$$

Generally, the JB moments depend on τ and τ'.

Eqs. (5)–(8) indicate that in the case of JB dipolar signal, the JB second moment $M_{2(\mathrm{JB})}$ can be related to the initial slope of the signal [1,7]. Since the normalization factor $S_{\mathrm{A}}\tau$ is given by the area under the JB dipolar signal,

$$S_{\mathrm{A}}\tau = \int_0^{\infty} S(\tau, \tau', t)\, \mathrm{d}t, \tag{9}$$

the JB second moment can be evaluated as [7]

$$M_{2(\mathrm{JB})} = \left| \lim_{t\to 0} \frac{\partial S(\tau, \tau', t)}{\partial t} \right| \Big/ \int_0^{\infty} S(\tau, \tau', t)\, \mathrm{d}t. \tag{10}$$

Unlike the usual second moment M_2 (powder average), the JB second moment $M_{2(\mathrm{JB})}$ cannot easily be calculated theoretically because the "weighting" factor $[-E^{\Omega}(\tau)R^{\Omega}(\tau')/\tau]$ is usually unknown. It is only shown [7] that the JB second moment $M_{2(\mathrm{JB})}$ reduces to the usual second moment M_2 in the limits of $(M_2^{\Omega})^{-1/2} \gg \tau$ and $T_{1\mathrm{D}}^{\Omega} \gg \tau'$.

However, the qualitative behavior of the τ dependent shape of the JB dipolar signal and hence of the τ dependent JB second moment $M_{2(\mathrm{JB})}$ can be seen by assuming a Gaussian function for the Zeeman FID signal. Namely, when $G^{\Omega}(\tau) = G_0 \exp(-M_2^{\Omega}\tau^2/2)$, the "weighting" factor becomes $\exp(-M_2^{\Omega}\tau^2/2)$. For simplicity, we have neglected the relaxation effect $R^{\Omega}(\tau')$ by assuming $T_{1\mathrm{D}}^{\Omega} \gg \tau'$. It is clear that for short τ satisfying $(M_2^{\Omega})^{-1/2} \gg \tau$, the "weighting" factor becomes independent of the crystal orientation, i.e., $M_{2(\mathrm{JB})} = M_2$. Also, the shape of the JB dipolar signal coincides with the time derivative of the shape of the Zeeman FID signal. For longer τ, the components of the JB dipolar signal with larger M_2^{Ω} may be suppressed in accordance with $\exp(-M_2^{\Omega}\tau^2/2)$ and the components with smaller M_2^{Ω} are relatively enhanced. This results in the JB dipolar signal relatively expanded in time. The $M_{2(\mathrm{JB})}$ value estimated by using the expanded signal will correspondingly be smaller, i.e., the $M_{2(\mathrm{JB})}$ value decreases with increasing τ. Such τ dependence of the $M_{2(\mathrm{JB})}$ can thus reflect the distribution of the M_2^{Ω} value due to the crystal orientation dependence in the powder sample.

Analysis of the τ dependence would elucidate detail of the M_2^{Ω} distribution, which is potentially useful as a new image contrast. But, it is not easy to perform such an analysis because a priori knowledge of the M_2^{Ω} distribution is required. Nevertheless, by using the "weighting" factor of $\exp(-M_2^{\Omega}\tau^2/2)$ and simply assuming a uniform M_2^{Ω} distribution which is symmetric about $M_2^{\Omega} = M_2$ and has the half range of the distribution ΔM_2^{Ω}, the τ dependence would be related to the half distribution range ΔM_2^{Ω}. Thus, the measurement of $M_{2(\mathrm{JB})}$ would allow an approximate measure of the M_2^{Ω} distribution range to be obtained, in addition to the usual powder average M_2.

As noted in the case of the Zeeman experiment, the presence of molecular motions may ruin the validity of Eqs. (5)–(10). However, we assume here that the motions are much faster or slower than the correlation times relevant to the JB experiment, so that the effective time-averaged dipolar Hamiltonian can safely be used for the rigid-lattice dipolar Hamiltonian [6]. Note that the whole shape of the JB dipolar signal is necessary for the second moment evaluation. Therefore, for performing the JB second moment imaging, the whole dipolar signal must be spatially resolved. This is in contrast to the second moment imaging based on the Zeeman signal, where only the initial curvature of the FID signal is required.

Fig. 1 shows the pulse sequence for the second moment 1D imaging using the JB dipolar signal. For imaging, the time evolution of the signal is suspended at a time t after the monitoring $45°_y$ pulse by the application of the magic echo time-suspension sequence, TREV-16TS [8–17]. Appropriate application of field gradient pulses (g) imposes the imaging evolution. Signal sampling (A/D) at even-numbered magic echo peaks [8–17] allows the imaging detection. The time t is scanned to cover the whole evolution of the JB dipolar signal. One-dimensional Fourier transformation along the time axis representing the imaging detection converts the

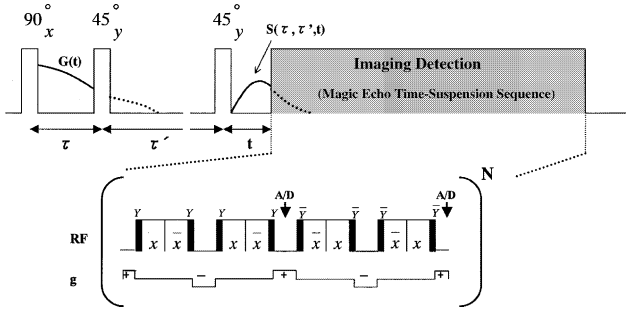

Fig. 1. Pulse sequence for second moment 1D imaging using the Jeener–Broekaert (JB) dipolar signal. The pair of pulses, $90°_x$–$\tau - 45°_y$, creates the dipolar order. The amplitude of the order decays during the following time interval τ' due to the spin–lattice relaxation with the time constant, $T_{1\mathrm{D}}$, and is then monitored by the application of a second $45°_y$ pulse. The signal, $\langle I_y \rangle$, induced immediately after the second $45°_y$ pulse assumes an "echo-like" shape and is called the JB dipolar signal, $S(\tau, \tau', t)$. For imaging, the time evolution of the signal is suspended at a time t after the monitoring $45°_y$ pulse by the application of the magic echo time-suspension sequence, TREV-16TS [8–17]. Appropriate application of field gradient pulses (g) imposes the imaging evolution. The pulse cycle of the TREV-16TS sequence is repeated N times; typically $N = 16$. Signal sampling (A/D) at even-numbered magic echo peaks [8–17] allows the imaging detection. The time t is scanned to cover the whole evolution of the JB dipolar signal.

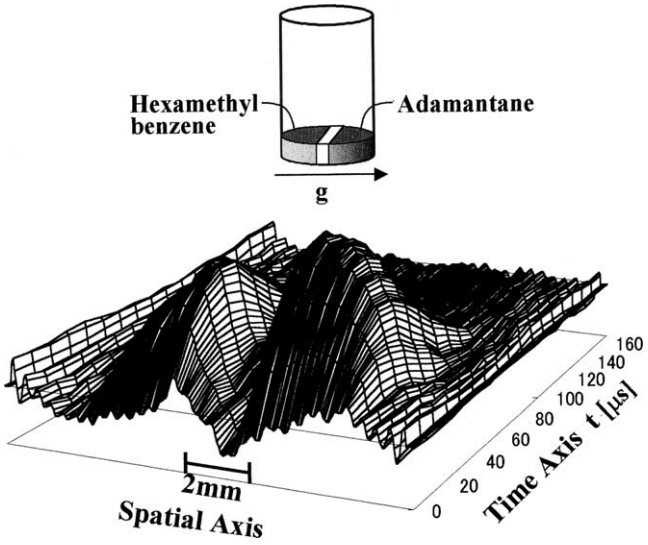

Fig. 2. Example of spatially 1D resolved JB dipolar signals obtained for the test sample consisting of adamantane (ADAM) and hexamethylbenzene (HMB) powders as shown by the inset. The 2D data acquired with the pulse sequence shown in Fig. 1 were converted by 1D Fourier transformation along the time axis representing the imaging detection to give this example. It corresponds to the experimental result shown in Fig. 5b. The initial slopes and the areas under the signals (Eqs. (10) and (9)) can be extracted from such converted 2D data with 1D spatial resolution, permitting the second moment imaging using the JB dipolar signal. Due to our instrumental restriction and the finite pulse width, the JB dipolar signals could not be acquired at exactly $t = 0$.

obtained 2D data to the spatially 1D resolved JB dipolar signals as illustrated in Fig. 2. The initial slope and the area under the signal, which corresponds to the spin density, can be extracted from such converted data at each resolved location based on Eqs. (10) and (9), permitting the second moment imaging using the JB dipolar signal. For improving the signal-to-noise ratio, the initial portion of the JB dipolar signals should be sampled more densely than the illustration, as we will do below.

3. Results and discussion

To confirm the theoretical expectations mentioned in the previous section, we have performed both non-imaging and imaging experiments by using mainly adamantane (ADAM) and hexamethylbenzene (HMB) powders. The usual second moments M_2 of these powders were measured previously from their dipolar spectra; namely, $M_2 = 0.94$ and $2.01\,\mathrm{G}^2$, respectively [4,5]. The transverse relaxation times are approximately the same: $T_2 = 50\,\mu\mathrm{s}$. The dipolar relaxation times T_{1D} are about 600 ms for ADAM and 50 ms for HMB.

We have first examined whether the shape of the JB dipolar signal depends on τ, and confirmed that the JB dipolar signal shape of HMB indeed depends on τ while the shape of ADAM essentially does not. This is shown in Fig. 3: As expected, the longer the spacing τ becomes, the more the HMB signal shape is expanded in time. The fact that ADAM does not clearly show such τ dependence can be explained by considering its molecular mobility. Further detail will be described later in this section. The τ dependence of the JB dipolar signal shape similar to HMB was observed in other organic samples like ferrocene, glycine, hydroquinone, adipic acid, and polycarbonate as well; the degree of the τ dependence was somehow different from sample to sample. The relaxation time $T_{1\mathrm{D}}$ of every sample was sufficiently long compared to the time interval τ', which was set at about $5T_2$, making the effect of the relaxation term $\exp[-\tau'/T_{1\mathrm{D}}^{\Omega}]$ on the JB dipolar signal negligible.

It is also expected that the JB second moment $M_{2(\mathrm{JB})}$ estimated from the initial slope of the normalized JB dipolar signal (Eq. (10)) depends on τ. The τ dependence of the $M_{2(\mathrm{JB})}$ is plotted in Fig. 4. It can be seen that for both ADAM and HMB, the $M_{2(\mathrm{JB})}$ values are close to the predetermined M_2 values of 0.94 and $2.01\,\mathrm{G}^2$ when τ is short. Further, for HMB, the $M_{2(\mathrm{JB})}$ value decreases with increasing τ, though it is nearly constant for ADAM. These observations are again consistent with the theoretical expectations, implying that the τ dependence reflects the distribution of the M_2^{Ω} value due to the crystal orientation dependence in the powder sample. The extraordinary weak τ dependence for ADAM can be explained by considering its molecular mobility. The isotropic molecular reorientation considerably diminishes the crystal orientation dependence [18]. See the detailed discussion on the molecular mobility later in this section.

The aforementioned simple analysis has been made on the τ dependence of the $M_{2(\mathrm{JB})}$ values: We have made the least squares theoretical fitting by using the Gaussian FID of $G^{\Omega}(\tau) = G_0 \exp(-M_2^{\Omega}\tau^2/2)$ and assuming a uniform M_2^{Ω} distribution. The uniform distribution was further assumed to be symmetric about $M_2^{\Omega} = M_2$. Although the M_2 can be included as an additional fitting parameter, the powder average M_2 was fixed in the theoretical fitting.

The theoretical τ dependence obtained for HMB is shown by the curve in Fig. 4, giving a value of $11.9\,\mathrm{G}^2$ for the half distribution range ΔM_2^{Ω}. The M_2 was fixed at $2.01\,\mathrm{G}^2$. Since the full variation of the M_2^{Ω} value must generally be smaller than $5M_2 = 10.1\,\mathrm{G}^2$ [6], the value of $11.9\,\mathrm{G}^2$ seems to be too large. Further, it gives some negative values for M_2^{Ω}. Also, for HMB, the experimental τ dependence exhibits an exponential character and markedly deviates from the theoretical τ dependence. These discrepancies may be mainly ascribed to the fact that the assumed distribution was over-simplified. The third discrepancy may be partly attributed to the fact that the dipolar spectrum of HMB looks like a Lorenzian while that of ADAM is well represented by a

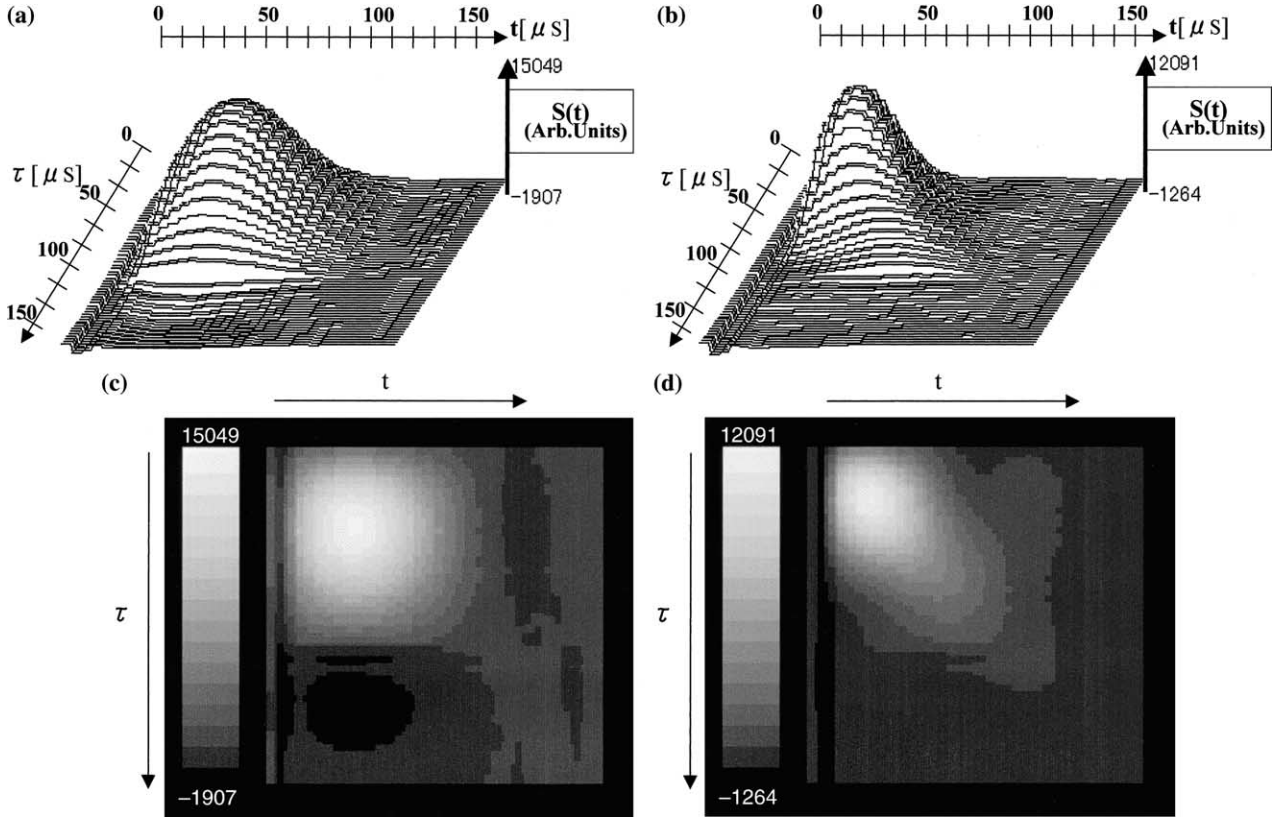

Fig. 3. The τ dependence of JB dipolar signals for (a) ADAM and (b) HMB samples. For clarity, the stacked plots (a) and (b) are also displayed as the gray-scale representations (c) and (d), respectively. These results were obtained by directly sampling the JB dipolar signals every 5 μs using 34 points. The initial 15 μs portions of the signals are obscured by the receiver dead time. The pulse spacing τ was incremented from 0 to 160 μs every 5 μs. While the HMB signal shape clearly depends on τ, the ADAM exhibits essentially no τ dependence. This can be explained by considering the molecular mobility in HMB and ADAM.

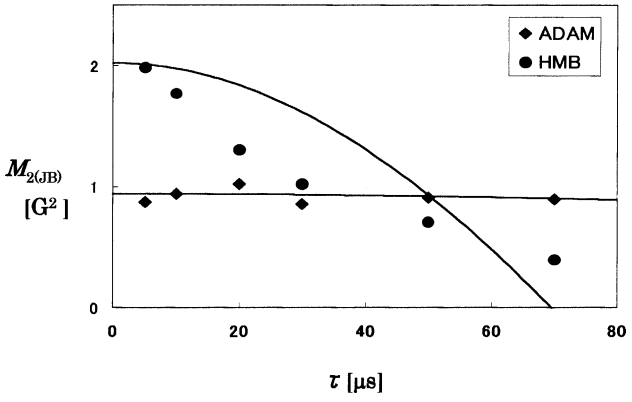

Fig. 4. Plots of the τ dependence of the JB second moment $M_{2(JB)}$ for ADAM and HMB. The τ dependence reflects the distribution of the M_2^{Ω} value due to the crystal orientation dependence in the ADAM and HMB powder samples. A simple analysis of the τ dependence yields an approximate value for the half distribution range ΔM_2^{Ω}. Solid lines show the least squares theoretical fits obtained by the analysis (see text for further detail). The experimental plots were obtained indirectly by sampling the second magic echo peak for avoiding receiver dead time of ca. 15 μs. The JB dipolar signal was sampled every 2 μs between $t = 0$ and 16 μs, and every 10 μs between $t = 20$ and 170 μs. The initial portion was sampled densely for improving the signal-to-noise ratio. While for HMB the JB second moment depends on the pulse spacing τ, it remains nearly constant for ADAM. This can be explained by considering the molecular mobility in HMB and ADAM.

Gaussian. The Gaussian FID assumed was not suitable for HMB, but appropriate for ADAM. The same fitting has been made for ADAM with the M_2 fixed at $0.94\,G^2$. The nearly straight line in Fig. 4 shows the theoretical τ dependence obtained for ADAM, signifying the much narrower distribution range. It yields a reasonable value of less than $0.05\,G^2$ for ΔM_2^{Ω}.

The simple analysis involves those serious problems and obviously more elaborated analysis is needed particularly for HMB; however, the preliminary results obtained through the simple analysis clearly corroborate that the observed variation of the τ dependent $M_{2(JB)}$ value can be correlated with the distribution range. Such information cannot be obtained from the Zeeman FID without using a single crystal.

The measurement of the JB second moment $M_{2(JB)}$ is now combined with the imaging experiment. We have conducted spatially 1D imaging experiments of the $M_{2(JB)}$ on a test sample consisting of ADAM and HMB powders (Fig. 2). The experimental results are summarized in Fig. 5. The $M_{2(JB)}$ images are displayed together with the spin density images (projections) for the three cases where the pulse spacing τ was set at (a) 15, (b) 30,

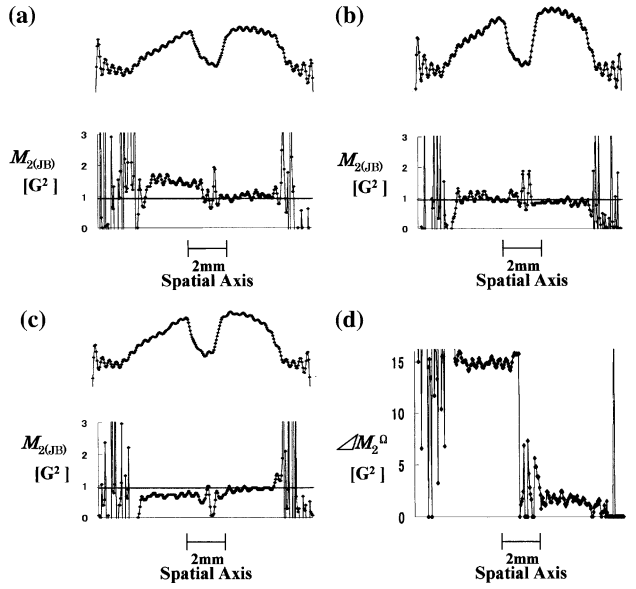

Fig. 5. Spatially 1D second moment images obtained for the test sample shown by the inset in Fig. 2. The JB second moment $M_{2(JB)}$ images are shown, together with the corresponding spin density images, in (a), (b), and (c) where the pulse spacing τ was set at 15, 30, and 50 μs, respectively. Note that, as in Fig. 4, while for HMB (left side) the localized $M_{2(JB)}$ clearly depends on the pulse spacing τ, it remains nearly constant for ADAM (right side). The spatially 1D image of the half distribution range ΔM_2^{Ω} is shown in (d), which was obtained by analyzing the spatially 1D resolved τ dependence deduced from the three $M_{2(JB)}$ images (a), (b), and (c). For ADAM on the right side of image (d), the M_2 value was fixed in the analysis at $0.8\,G^2$ rather than at $0.94\,G^2$ for achieving a better least squares fitting (see text for further detail). The localized ΔM_2^{Ω} values are somewhat larger than the non-localized values of $11.9\,G^2$ and less than $0.05\,G^2$ for HMB and ADAM. The t scanning to cover the JB dipolar signal evolution was also the same as in Fig. 4.

and (c) 50 μs. As in Fig. 4, it can be noted that while for HMB on the left side of projection the $M_{2(JB)}$ clearly depends on τ, it remains nearly constant around the predetermined M_2 value of $0.94\,G^2$ [4,5] for ADAM on the right side of projection. The same analysis as in Fig. 4 has been made on the spatially 1D resolved τ dependence obtained from the three $M_{2(JB)}$ images (a), (b), and (c). This has yielded the spatially 1D image of the half distribution range ΔM_2^{Ω} shown in Fig. 5d. The localized ΔM_2^{Ω} values are somewhat larger than the non-localized values of $11.9\,G^2$ and less than $0.05\,G^2$ for HMB and ADAM. For ADAM, a better fitting was achieved with $M_2 = 0.8\,G^2$ rather than with $M_2 = 0.94\,G^2$. All these discrepancies between the non-localized and localized results may probably be attributed to the least squares fitting made on the poor localized data for the τ dependence, which is represented by only three points. Despite the discrepancies, the preliminary results shown in Fig. 5 clearly demonstrate the feasibility and the potential utility of the JB second moment imaging in materials characterization.

The fact that ADAM does not clearly show the τ dependence may be explained by considering the molecular mobility. In the ADAM sample, the rapid isotropic reorientation of the nearly spherical ADAM molecules averages out the intramolecular dipolar interaction and only the intermolecular dipolar interaction survives [18]. Generally, while the lattice sum of the intramolecular dipolar interaction is highly orientation dependent, that of the intermolecular dipolar interaction is expected to be much less orientation dependent. This may lead to the extraordinary weak τ dependence of the JB second moment for ADAM. Although the HMB molecules similarly undergo reorientation about the C_6 axis in addition to the methyl reorientation [18], the reorientations are not isotropic. This makes the intramolecular dipolar interaction survive, resulting in the much stronger τ dependence of the JB second moment for HMB.

Although the τ dependence of the JB second moment observed for the organic samples was ascribed only to the crystal orientation dependence, another mechanism may also be responsible for the τ dependence observed, for example, in the polycarbonate sample. As is well known, most polymers exhibit heterogeneities of molecular mobility, which can give rise to an additional distribution of the second moment. Therefore, to the extent that spin diffusion can be neglected, the heterogeneities can contribute to the τ dependence. Further examination is the purpose of our next study.

4. Conclusion

We have demonstrated that imaging of the ^1H NMR second moment can be achieved by using the JB dipolar signal instead of the Zeeman signal commonly employed. The JB dipolar signal was induced by applying a JB pulse sequence, $90°_x$–$\tau - 45°_y$–$\tau' - 45°_y$, which was followed by the time-suspension magic echo sequence, TREV-16TS, for imaging detection. Scanning the imaging detection to cover the whole evolution of the JB dipolar signal resulted in producing spatially resolved JB dipolar signals. The local value the JB second moment $M_{2(JB)}$ was then estimated from the initial slope of each resolved JB dipolar signal.

The JB second moment $M_{2(JB)}$ can be regarded as the "weighted" powder average of the usual second moment M_2^{Ω}. The "weighting" effect results in the τ dependence of the JB second moment $M_{2(JB)}$, from which the approximate range of the M_2^{Ω} distribution due to the orientation dependence can be deduced in addition to the usual powder average of the second moment M_2. These theoretical expectations have been confirmed by both non-imaging and imaging experiments performed on the test samples of ADAM, HMB, and some other organic powders. The parameters characterizing the M_2^{Ω}

distribution, such as the distribution range are potentially useful for new contrasts in materials imaging. This has been demonstrated by the preliminary imaging experiments performed on the test sample.

5. Experimental

All the experiments were performed on a homebuilt NMR imager, operating at 59.85 MHz for protons. The 90° pulse length was 2.4 μs. The JB pulse spacing, τ', for attaining the internal equilibrium was set at least 5 times as long as the relaxation time T_2 of the sample under measurement (Fig. 1). The cycle time of the magic echo time-suspension sequence, TREV-16TS [8–17], was fixed to 1.2 ms. For example, under these conditions, the decay constant of the latter half of the ADAM dipolar signal, ~35 μs, was increased to ~10 ms by the application of the TREV-16TS sequence.

The gradient amplitude was 1.6 G/cm, giving an FOV of about 9 mm. Thirty-two points were sampled during the imaging detection (Fig. 1) and zero-filled to 256 points before the Fourier transformation. The amplitudes of the JB dipolar signals were about 4–5 times smaller than those of the corresponding Zeeman signals and hence signal accumulation of 8–32 was made.

We confirmed that the τ dependence shown in Figs. 3–5 remained unchanged even if the pulse spacing τ' was increased up to 20 ms from 250 μs.

Acknowledgments

We thank Prof. Shigehiko Yamamoto of University of Tsukuba for encouragement. Thanks are also due to Prof. Kiyonori Takegoshi of Kyoto University for helpful discussions on the τ dependence, Dr. Masayuki Nonaka of Hitachi Medical Corporation, and Ms. Hiroko Hirayama of University of Tsukuba assisted some of the data processing.

References

[1] J. Jeener, P. Broekaert, Phys. Rev. 157 (1967) 232–240.
[2] A.G. Anderson, S.R. Hartman, Phys. Rev. 128 (1962) 2023–2041.
[3] F. Weigand, D.E. Demco, B. Blümich, H.W. Spiess, Solid State NMR 6 (1996) 357–365.
[4] S. Matsui, M. Nonaka, T. Nakai, T. Inouye, Solid State NMR 10 (1997) 39–44.
[5] M. Nonaka, S. Matsui, T. Inouye, J. Magn. Reson. 145 (2000) 315–318.
[6] A. Abragam, The Principles of Nuclear Magnetism, Oxford University Press, London, 1961.
[7] M. Bloom, E.E. Burnell, S.B.W. Roeder, M.I. Valic, J. Chem. Phys. 66 (1977) 3012–3020.
[8] S. Matsui, Chem. Phys. Lett. 179 (1991) 187–190.
[9] S. Matsui, J. Magn. Reson. 95 (1991) 149–153.
[10] S. Matsui, J. Magn. Reson. 98 (1992) 618–621.
[11] S. Matsui, Y. Ogasawara, T. Inouye, J. Magn. Reson. A 105 (1993) 215–218.
[12] S. Matsui, A. Uraoka, T. Inouye, J. Magn. Reson. A 112 (1995) 130–133.
[13] S. Matsui, A. Uraoka, T. Inouye, J. Magn. Reson. A 120 (1996) 11–17.
[14] S. Matsui, M. Nonaka, T. Nakai, T. Inouye, J. Magn. Reson. 138 (1999) 220–224.
[15] F. Weigand, B. Blümich, H.W. Spiess, Solid State NMR 3 (1994) 59–66.
[16] M.L. Buszko, G.E. Maciel, J. Magn. Reson. A 107 (1994) 151–157.
[17] M.A. Hepp, J.B. Miller, J. Magn. Reson. A 111 (1994) 62–69.
[18] S.J. Kitchin, K.D.M. Harris, A.E. Aliev, D.C. Apperley, Chem. Phys. Lett. 323 (2000) 490–497, and references therein.